EURASIP Journal on Applied Signal Processing 2002:10, 1053–1066

Image-Based Multiresolution Implicit Object Modeling

Augusto Sarti
Dipartimento di Elettronica e Informazione, Politecnico di Milano, Piazza L. Da Vinci 32, 20133 Milano, Italy
Email: sarti@elet.polimi.it

Stefano Tubaro
Dipartimento di Elettronica e Informazione, Politecnico di Milano, Piazza L. Da Vinci 32, 20133 Milano, Italy
Email: tubaro@elet.polimi.it

Received 5 October 2001 and in revised form 14 May 2002

We discuss two image-based 3D modeling methods based on a multiresolution evolution of a volumetric function's level set. In the former method, the role of the level set implosion is to fuse ("sew" and "stitch") together several partial reconstructions (depth maps) into a closed model. In the later, the level set's implosion is steered directly by the texture mismatch between views. Both solutions share the characteristic of operating in an adaptive multiresolution fashion, in order to boost up computational efficiency and robustness.

Keywords and phrases: object modeling, 3D reconstruction, level-set, surface reconstruction, multi-base-line stereo.

1. INTRODUCTION

Building a complete 3D model of objects from a sequence of images is a task of great difficulty, as it involves many complex steps such as camera motion tracking, image-based depth estimation, and global surface modeling. In order to solve the first problem, a variety of solutions are available either in the literature or commercially. Aside from the many motion feedback systems available in commerce, the literature is rich with image-based systems that enable a fairly reliable estimation of the camera motion through the analysis of the acquired video sequences. Such solutions usually exploit projective constraints and invariants to perform image calibration [1] and vary in how such constraints are used, how the outliers are managed, and whether additional information (feature coplanarity, collinearity, etc.) can be included. Alternative camera motion estimation techniques are based on Extended Kalman Filtering and are also available commercially and in the literature [2, 3] in more or less sophisticated versions. In this paper, we will not be concerned with the problem of camera motion estimation, instead, we will focus on the problem of global surface modeling based on images.

With "global surface" we mean the external (visible) frontier of a volume, which is bound to be a closed surface. Modeling closed surfaces, indeed, poses a number of representation problems which are typical of differential topology. Such surfaces, in fact, can be thought of as differentiable manifolds, and their modeling solutions are closely related to their classical representations.

A 3D manifold can be generally defined and represented either *explicitly*, through a juxtaposition of overlapping 3D maps; or *implicitly*, as the set of points that satisfy a nonlinear constraint in the 3D space (a level set of a volumetric function). Using the former or the latter, surface representation has a substantial impact on how the image-based 3D modeling problem is posed. An explicit global object model is, in fact, obtained as a "patchworking" of local reconstructions (range images or depth maps), while an implicit surface is described as a level set of an appropriate volumetric function. An explicit modeling method deals with topological complexity with a "divide-and-conquer" strategy, which simplifies the local shape estimation process. The price to pay for this simplification, however, is in the complexity of the steps that are necessary for fusing the local reconstruction into a global closed one (registration, fusion and hole-mending). An implicit approach to surface modeling, on the other hand, tends to be more robust against topological complexity, as it may easily accommodate self-occluding surfaces, concavities, arbitrary topological varieties (e.g., doughnut-shaped surfaces, objects with handles, etc.), or even multiple objects. On the other hand, an implicit method is bound to work with volumetric data, with more storage requirements and a heavier computational load.

Level set methods were first proposed in [4] by Sethian, as a powerful approach to the modeling of evolving inter-

faces in a variety of fields, ranging from computational geometry to materials science [5]. The approach has been studied in depth over the past two decades and a variety of solutions have been proposed to overcome some of the basic limitations of the method and to make it as computationally efficient as possible. More recently, the level set approach proved effective for several image processing and computer vision applications [6, 7, 8, 9, 10, 11, 12, 13], including image-based 3D surface modeling [14]. In particular, some effective strategies have been proposed to overcome the inevitable computational costs associated to the intrinsic volumetric representation in image-based shape modeling. Such solutions refer to two different approaches to image-based surface modeling: the first (indirect method) consists of constructing the global surface as 3D mosaic of simpler surface patches [15], while the second (direct method) skips the partial modeling step and uses the available images to steer the evolution of the level set toward the final surface shape [16]. Both methods use a narrow-band approach in conjunction with a multiresolution technique (adaptive cell size) to boost the performance of surface fusion and image-based 3D modeling techniques. In this paper, we will explore these two methods in depth, discussing the fundamental differences in their implementation strategies and illustrating some implementational aspects of the solutions.

In Section 2, we review some well established basic ideas behind implicit object modeling in the context of image-based surface modeling applications. The purpose of this section is to provide the readers who are not familiar with implicit methods with some helpful ideas to better understand the rest of this contribution . In Section 2, we also anticipate some technical solutions that we adopted in the specific applications described in the following two sections. In Section 3, we propose a novel application of the ideas set forth in Section 2 to the surface fusion problem. In particular, we discuss how to specialize the front evolution for this particular application and how to obtain optimal performance from this approach, both in terms of quality of the results and in needed computational power. Section 4 addresses in depth a second image-based modeling application where front evolution is directly driven by images. Although the approach used for this second application is not new [14], the solutions adopted to boost the performance and cut the computational cost of this implementation are new. This method, in fact, allows to operate in a multiresolution fashion. In particular, a careful management of front evolution is proposed, which is able to back-track and recover details lost at lower levels of grid density. Applications to real data are presented in each section, which prove the effectiveness of the approach. Final comments and proposals of improvements conclude this contribution in Section 5.

2. IMPLICIT SURFACE MODELING

As already discussed in Section 1, although there are a variety of reasons why an implicit surface representation would be preferable over an explicit one, the most compelling reasons remain the ability to deal with complex surface topologies and the optimal and simultaneous management of the available image information. In this section we provide the reader with some fundamentals on level set evolution in the context of image-based modelling applications.

2.1. Interface propagation

Our approach to surface modelling is not through piecewise construction, but through interface propagation, that is, the temporal evolution of a closed oriented surface or, more generally, of some oriented surface that separates two regions from each other. This surface will "sweep" the volume of interest until it takes on the desired shape under the influence of some properly defined action.

Since we are not interested in any interface motion in its own tangential directions, we can assume this surface to move in a direction normal to itself (either outward or inward) with a known velocity function F. It is in this speed function that we will embed the external action terms, plus the necessary smoothing terms that guarantee a successful convergence of the front to the desired solution. The velocity function, in general, depends on a variety of information sources, which are more or less related to the shape of the front [5], as follows.

Local (intrinsic) properties of the front: local geometric information on the front, such as curvature and normal direction.

Global properties of the front: global information that depends on the available data, and that usually depends on the shape and the position of the front (through integration over the front).

Independent properties: external action terms that are independent of the shape of the front.

A proper choice for the velocity function is crucial for the success of the modeling technique. Later in this section we will illustrate some examples of properties that we used for our applications to 3D surface modeling.

There are two distinct formulations of the differential equations that describe interface motion. The first is referred to as boundary value approach, and the second is the initial value approach. Such formulations lead to the fast marching method and the level set method, respectively.

2.1.1 Boundary value approach

If we can assume that the velocity term F is always positive, the characterization of the position of the front $\Gamma(t)$ can be entirely given in terms of the arrival time $T(\mathbf{x})$ of the front as it crosses each point $\mathbf{x} = [x_1 \;\; x_2 \;\; x_3]^T$,

$$\Gamma(t) = \{\mathbf{x} \mid T(\mathbf{x}) = t\}. \tag{1}$$

The gradient ∇T of this function is bound to be orthogonal to its level sets, therefore it is parallel to the velocity function F. If we also consider the usual idea that velocity is the ratio between displacement and time, then the arrival function T will satisfy the equation

$$|\nabla T| F = 1, \tag{2}$$

where we have $T = 0$ on the initial location $\Gamma(0)$ of the interface. We thus have a formulation of the problem in terms of a PDE (partial differential equations) subject to a boundary condition [5].

2.1.2 Initial value approach

If we want to remove the constraint of monotonic propagation and allow the front to move forward and backward, then the crossing time T can no longer be a single-valued function. We thus need to adopt an alternative representation for the front. An appropriate choice is to represent the initial front as the zero level set of a volumetric function ϕ. We can then link the evolution of this function to the propagation of the front through a time-dependent initial value problem [8, 9, 10, 17]. The front, in fact, will be given by

$$\Gamma(t) = \{\mathbf{x} \mid \phi(\mathbf{x}, t) = 0\}. \tag{3}$$

The equation of the motion can be easily derived by imposing that a particle on the front with trajectory $\mathbf{x}(t)$ lies on the zero level set of the volumetric function

$$\phi(\mathbf{x}(t), t) = 0, \tag{4}$$

and that the normal component of its velocity matches F

$$\frac{\partial \mathbf{x}(t)}{\partial t} \cdot \mathbf{n} = F, \tag{5}$$

where $\mathbf{n} = \nabla\phi/|\nabla\phi|$.

Differentiating the left-hand side of (4)

$$\frac{\partial \phi}{\partial t} + \frac{\partial \mathbf{x}(t)}{\partial t} \cdot \nabla\phi = \frac{\partial \phi}{\partial t} + \frac{\partial \mathbf{x}(t)}{\partial t} \cdot \mathbf{n}|\nabla\phi|, \tag{6}$$

and using (5), the initial value problem [17] can be rewritten as

$$\frac{\partial \phi}{\partial t} + F|\nabla\phi| = 0, \tag{7}$$

given $\phi(\mathbf{x}, 0)$. Equation (7) can be discretized into the update equation

$$\phi(\mathbf{x}, t + \Delta t) = \phi(\mathbf{x}, t) - \left|\nabla\phi(\mathbf{x}, t)\right| F(\mathbf{x})\Delta t. \tag{8}$$

It is important to emphasize the fact that now there is no a priori condition on F, which can be arbitrary. In particular, its sign is free to change, therefore the front can move forward and backward as it evolves. This particular PDE becomes a special case of the Hamilton-Jacobi equation if the speed depends only on position $\mathbf{x}$ and first derivatives of ϕ.

In applications of computer vision and 3D modeling, the structure of the embedding volumetric function ϕ is not naturally suggested by the nature of the problem, therefore we can invoke the need to keep computations as simple as possible and decide on a volumetric function whose absolute value in $\mathbf{x}$ is given, the distance d between $\mathbf{x}$ and the evolving front and its sign depends on whether the point $\mathbf{x}$ is inside or outside the surface. Adopting the signed distance as a volumetric function, in fact, simplifies the computation of the surface's differential properties [5] of orders 1 and 2:

(i) the surface normal can be computed as the gradient $\nabla\phi$ and is a unit vector;

(ii) the surface curvature can be computed as a divergence of the form $\nabla \cdot \nabla\phi$.

2.1.3 A comparison

It is important to notice that (2) requires $F > 0$ all the time, which means that the front is expected to move always in the same direction, because it must generate one single crossing time per grid point (points cannot be revisited). This is, indeed, a very strong requirement that should be avoided in image-driven surface shaping schemes, especially if working in with variable grid resolution. In fact, if we happen to miss some surface details at a certain grid resolution, we need to be able to backtrack the evolution and retrieve the lost details as we increase its resolution.

Also, the framework of initial value level set methods allows to define the speed function in a quite arbitrarily complex fashion. This gained freedom, however, has a price in terms of computational efficiency. Fast marching methods, which are efficient implementations of boundary value methods, benefit from the fact that the time of arrival is a single-valued map to compute the front evolution in a single sweep, using heap-sort algorithms to generate the grid's visiting order. In spite of the loss of efficiency, level set methods, which are direct implementations of initial value solutions, can be made quite efficient through a joint use of narrow band and adaptive mesh strategies [5]. Because of these reasons, and others that will be illustrated throughout the paper, we adopt a level set approach for our surface modeling solutions.

2.2. Front stability and smoothness

Before we begin illustrating our approach to steering the level set evolution using images, some clarifications on the stability and the correctness of the front propagation are in order. As a matter of fact, deciding on a reasonable velocity function may be a problem if we do not include some sort of smoothness term. For example, a front evolving at constant speed may easily develop unwanted corners and become nondifferentiable. In order to proceed with the front propagation we must search for a weak solution for the propagating front (meaning that it satisfies an integral formulation of the differential equation). Similarly, in some cases we could have ambiguities in how to continue front propagation (gaps in the solutions). Such problems can be safely solved by introducing in the velocity function a smoothing term that is proportional to the local curvature of the front. When the velocity's magnitude is proportional to the local curvature, the front evolution is said to follow a motion by curvature. As we can see in Figure 1, if this motion is uncontrasted, it tends to smoothen more and more the initial shape as the front evolves. There is, however, an important result in the theory of level set evolution that states and proves that the correct result (entropy solution) can be achieved as the limit of the smooth solution as the smoothing term goes to zero [5].

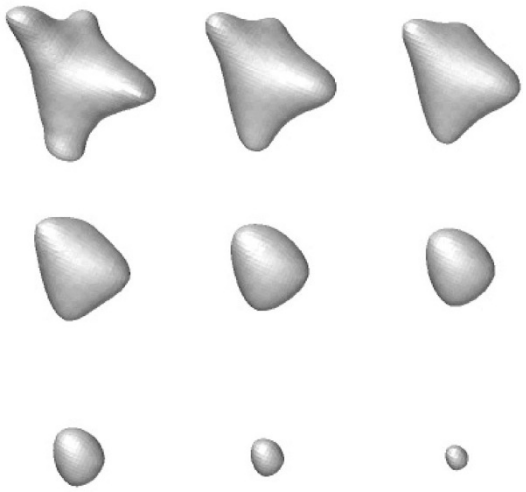

Figure 1: Motion by curvature: the surface deflates in a maximally smooth fashion until it disappears.

The necessity of a smoothing term is also justified by the need of overcoming the intrinsic ill-conditioning of stereo problems and, more generally, of computer vision problems.

2.3. Narrow band

Updating the volumetric function whose level set zero represents the propagating front requires, in principle, the updating of $O(M^3)$ voxels, M being the linear size of the voxset (expressed in voxels). A Lagrangian (particle tracking) approach, on the other hand, is only expected to update the location of the points of the propagating front, therefore we only need to act on $O(M^2)$ points. This excess in the computational cost associated to a level set approach is due to the intrinsic redundancy of an implicit surface representation, but it can be drastically reduced if we consider that the volumetric function ϕ does not need to be updated everywhere, as we are only interested in the zero level set of ϕ. In fact, only the values of ϕ in the proximity of the front tend to have an influence on the evolution of its shape, due to the spatial derivatives that appear in the PDE that governs the front propagation. As a consequence, it is possible to limit the region of influence to a "narrow band" (NB) centered around the evolving front

$$\mathbf{x} \in NB \iff |\phi(\mathbf{x})| \leq \frac{\delta}{2}, \tag{9}$$

δ being the thickness of the narrow band [12, 18]. As a consequence, the number of voxels to be updated is back to $O(M^2)$. We have to keep in mind, however, that the inevitable discretization errors that occur in the implementation of the equation that governs the front evolution require an occasional reinitialization of the volumetric function within the narrow band, with the constraint of keeping the front unchanged. The choice of the thickness δ must be a trade-off between the need of minimizing the number of voxels to update and minimizing the number of reinitializations. Typically, δ is set to values that range between 10 and 20 voxels.

A straightforward way to implement the updating process for NB reinitialization is based on the recomputation of the distance function from the front. This operation, however, is computationally expensive, therefore we adopt an iterative approach to do so. The method consists of a first rough reinitialization of the volumetric function, followed by an iterative refinement process that returns the actual signed distance function from the front. This iterative process is meant to change the function in order for its gradient to have a unit magnitude. This is, in fact, done by discretizing a special type of Hamilton-Jacobi PDE [19],

$$\frac{\partial \phi}{\partial t} = \operatorname{sign}(\phi_0) \cdot (1 - |\nabla \phi|), \tag{10}$$

whose solution is a distance function ϕ ($|\nabla \phi| = 1$) and whose level zero is the initial function ϕ_0. This iterative scheme turns out to be far more efficient than a complete reinitialization, especially if the rough initialization ϕ_0 is already quite accurate [20]. One way to build a good approximation ϕ_0 of the desired function ϕ is to keep the previous values. Of course, as the front migrates between two reinitializations, we will be able to use only some of the previous values. The other voxels (those that are located in the new portions of the narrow band) will be assigned increasing (decreasing) values as we move outward (inward) with respect to the front.

This method [21] has been proven to be equivalent to the so called "upwind scheme" [5], which is based on an appropriate choice of the discretization of the partial differentiation operator.

2.4. Multiresolution

As already said above, working in a narrow band around the propagating front dramatically reduces the number of voxels to be updated from $O(M^3)$ to $O(M^2)$. A further drastic reduction in the updating complexity comes from the adoption of a multiresolution strategy in the front evolution, which drops the complexity to a mere $O(M \log M)$. The term multiresolution, however, requires some explanation, as it may lead to completely different solutions in the data structure and management. In particular, if we do not know in advance where the surface details are located (direct, or image-driven, shape modeling), all we can do is to let the front evolve on a coarse grid, and increase the voxset resolution of a factor two ($2^3 = 8$ smaller voxels for each coarser one) every time the front evolution comes to a stop (equilibrium configuration). When the location of the surface details is known (indirect, or surface-driven, modeling), we can do better than just perform an on-the-fly split of the whole voxset. In fact, we can reorganize the data structure in a hierarchical fashion using an octree. This, of course, complicates the computation and the management of the derivatives and of the velocity function, but it boosts the performance even further.

Aside from the data structure management, what deserves more investigation in this context is, in fact, how to deal with details that might not be captured at a lower resolution. This discussion, however, will be given in the two

applications (indirect and direct modeling) proposed in the next two sections.

2.5. Construction of the extension velocities

It is important to point out that the velocity function is usually defined only on the propagating front $\Gamma(t)$ (zero level set of ϕ). On the other hand, in order to be able to integrate the PDE that governs the motion of the propagating front, we need the speed function to be defined on the whole domain of interest of ϕ, which is the narrow band defined in Section 2.3. The extension of the velocity function in that domain must be done starting from its profile on the propagating front, in such a way to guarantee that the evolution of ϕ in the whole narrow band will be consistent with evolution of the propagating front [22]. Roughly speaking, we would like all level sets of ϕ to propagate without self-collisions (swallowtail configurations) or rarefactions (gaps).

In order to define an extension of the velocity function that does not generate self-collisions or rarefactions, we can proceed as follows: let $\Gamma = \{\mathbf{x} \mid \phi(\mathbf{x}) = 0\}$ be the propagating front and consider a generic point $\mathbf{x}_P$. If $\mathbf{x}_P$ does not lie on Γ, we can always find another level set that it belongs to. In other words, we can always find a c such that $\phi(\mathbf{x}_P) = c$. If

$$\mathbf{x}_Q = \arg\min_{\mathbf{x}_Q \in \Gamma} ||\mathbf{x}_Q - \mathbf{x}_P|| \tag{11}$$

is the closest point of Γ to $\mathbf{x}_P$, then we can assign $\mathbf{x}_P$ the velocity $F(\mathbf{x}_P) = F(\mathbf{x}_Q)$. This operation can be done for every point of the narrow band, and is exempt from the abovementioned problems of self-collision or rarefaction [5].

2.6. Volumetric and surface rendering

Visualizing the zero level set of a volumetric function is important when we need to visually follow the evolution of the front. Conventional surface visualization techniques, however, are suitable for Lagrangian surface descriptions (triangle mesh), but they do not directly apply to an implicit surface representation. In this section, we discuss a solution for visualizing the evolving front, without having to construct the surface mesh.

The method consists of assigning a luminance value to a generic pixel through the analysis of sign changes in the volumetric function ϕ along the associated optical ray:

(i) if the volumetric function $\phi(\mathbf{x})$ does not change sign along the optical ray, we assign the pixel the background luminance;

(ii) if $\phi(\mathbf{x})$ exhibits a sign change along the optical ray, then the pixel will be assigned a value of luminance, computed using an appropriate radiometric model that accounts for the viewing direction and the normal to the front. In fact, we assume the local texture to be locally uniform and the light to be diffused, the luminance will only depend on the viewing direction (non-Lambertian component)

$$I = \frac{\mathbf{i} \cdot \mathbf{n}}{\|\mathbf{i}\| \|\mathbf{n}\|}, \tag{12}$$

where $\mathbf{i}$ is the viewing direction and $\mathbf{n}$ is the front's normal in the considered point, which can be computed directly from the samples of ϕ that surround the point along the optical ray, where ϕ changes sign.

It is also quite easy to map other characteristics on the evolving front, such as the cost function or the original textures. As for the final model, the conversion to a more conventional wireframe can be easily performed using a modified *marching cubes* algorithm [23].

3. INDIRECT SURFACE MODELING

A common way to build a complete 3D object model consists of combining several simpler surface portions [24, 25, 26] (range images or depth maps) through a 3D "mosaicing" process. In order to do so, we need a preliminary registration phase [27], in which all the available surface patches are correctly positioned and oriented with respect to a common reference frame; and a fusion process, which consists of merging all surface patches together into one or more closed surfaces. One rather standard registration strategy is the Iterative Closest Point [28] algorithm, which consists of minimizing the mean square distance between overlapping portions of the surface, using an iterative procedure. As for surface fusion, in this section we propose and test an approach that is able to seamlessly "sew" the surface overlaps together, and reasonably "mend" all the holes that remain after surface assembly (usually corresponding to non-visible surface portions).

This patchworking process is suitable for combining 2D 1/2 modeling solutions such as image-based depth estimation techniques, range cameras, and laser scanners. It is important to stress that the depth maps produced by such devices could be made of several non-connected surface patches, as occlusions and self-occlusions tend to generate depth discontinuities [26]. Such surfaces usually need a lengthy assembly process in order to become a complete and closed surface.

3.1. Definition of the velocity function

The velocity function that steers the front evolution accounts for two contrasting needs: that of generating a smooth front propagation with no degenerate configurations (motion by curvature) and that of honoring the data (oriented surface patches). As already seen in the previous section, if the motion were purely by curvature, a surface would tend to deflate completely and disappear, while becoming progressively smoother and smoother (Figure 1). The need to honor the available range data prevents this complete implosion from taking place.

Let $\mathbf{x}$ be a point on the evolving front Γ, k the local curvature of the front in $\mathbf{x}$, and d the distance from $\mathbf{x}$ to the closest available surface. Our velocity function combines a term of the form $F_1(k)$, which promotes motion by curvature, with a term of the form $F_2(d)$, which encourages data fitting. In principle, there are several ways to do so. The most obvious choice of a simple product, however, tends to

produce unpleasant front profiles in the proximity of discontinuities between different surface portions. A better front behavior is obtained by replacing the product with a simple sum of the two above terms. This solution, however, tends to round all edges, with a consequent loss of accuracy. In order to avoid this problem, we define the velocity function as

$$F(\mathbf{x}) = F_1(k(\mathbf{x})) + \alpha \frac{k_M(\mathbf{x})}{k(\mathbf{x})} F_2(d(\mathbf{x})), \tag{13}$$

where k is the front's local curvature, k_M is the local curvature of the facing surface; d is the distance (with sign) between the propagating front and the surface patch; and α is a weight that balances the two terms of local smoothness and data fitting. In this version of the velocity function, the term that promotes data fitting is multiplied by a corrective factor that depends on the local curvature of the surfaces that are facing the front. This tends to encourage the front to fit the data much more in the proximity of edges.

Notice that the above definition of velocity is only valid on the propagating front, therefore we need to extend it to the whole volume of interest (narrow band around the propagating front), as explained in Section 2.3.

3.2. Precomputation of the distance function

One crucial step of the indirect method is the computation of the distance function that appears in (13), which characterizes the data-fitting term of the velocity function. The zero level set of this function gives a rough idea of the global shape and of the level of detail that the final model will have, therefore it allows to correctly decide initial and final spatial discretization steps. In fact, the initial voxset resolution must be sufficient to capture the topology of the surface to model, while the final voxset resolution must be adequate to model the surface details.

It is important to emphasize that the distance function can be computed on the whole volume of interest before starting the front evolution. Given a generic point $\mathbf{x}$, its distance from a single oriented surface can be easily computed as the distance between $\mathbf{x}$ and its projection onto the closest triangle of the mesh (Figure 2). If no point on the surface patch faces the point on the level set orthogonally, then the distance function d is computed from the closest point on the border of the patch (within certain angular limits). Of course this distance will be attributed a sign, depending on which side of the surface the point $\mathbf{x}$ is facing. In particular, negative values of the distance function tend to prevent the front from penetrating apertures or holes between surface portions and avoids useless concavities. Indeed, this computation leads to a distance whose zero level set coincides with the initial surface.

In the presence of several surfaces, the distance must be computed as a combination of the various distances (within reasonable limits), taking into account, somehow, their reliability. Indeed, a special case is represented by two overlapping surfaces that are oppositely faced, and need to be treated separately (in this case the viewpoints are in opposition).

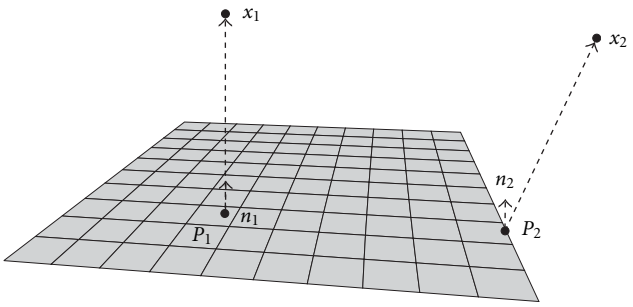

Figure 2: Distance function in the case of a single surface.

Also, we need to exclude all surface portions that, although correctly oriented, are too far apart from the considered point.

If we consider the kth mesh of triangles, $k = 1, \ldots, N$, we can compute the distance $d_k(\mathbf{x})$ from the point $\mathbf{x}$ as follows:

(1) find the closest node $\mathbf{m}$ to $\mathbf{x}$;
(2) find the point $\mathbf{p}$ that lies the closest to $\mathbf{x}$, on the triangles that share the node as a vertex;
(3) compute $d_k(\mathbf{x})$ as follows:
  (i) if $\mathbf{p}$ is not a frontier point of the triangle mesh, then $d_k(\mathbf{x}) = (\mathbf{x} - \mathbf{p}) \cdot \mathbf{n}$;
  (ii) if $\mathbf{p}$ is a frontier point of the triangle mesh, then

$$d_k(\mathbf{x}) = \begin{cases} +\left|(\mathbf{x} - \mathbf{p})\right| & \text{when } (\mathbf{x} - \mathbf{p}) \cdot \mathbf{n} \geq 0, \\ -\left|(\mathbf{x} - \mathbf{p})\right| & \text{when } (\mathbf{x} - \mathbf{p}) \cdot \mathbf{n} < 0. \end{cases} \tag{14}$$

The zero level set of $d_k(\mathbf{x})$ turns out to be continuous and piecewise linear, just like the original triangle mesh.

In order to compute the global distance function $d(\mathbf{x})$ that pertains a set of multiple surfaces, we can proceed as follows:

(1) find the algebraic distance $d_k(\mathbf{x})$, $k = 1, \ldots, N$, from each available mesh;
(2) if all distances correspond to border points, then let

$$d(\mathbf{x}) = d_{\min}(\mathbf{x}), \tag{15}$$

otherwise go to step 3.
(3) let $\hat{d}_{\min}(\mathbf{x})$ be the smallest of all distances $d_k(\mathbf{x})$ that are not measured from a border point. Let $\mathbf{p}_{\min}$ be the point from which that minimum distance is computed, $\mathbf{n}_{\min}$ be the surface normal at that point, and

$$I = \{k \mid (\mathbf{n}_k \cdot \mathbf{n}_{\min}) > 0\} \tag{16}$$

be the set of indices that identify all surfaces oriented like $\mathbf{n}_{\min}$, $\mathbf{n}_k$ being the normals at the other closest non-border points. Similarly, we can determine the set of surfaces oriented opposite to $\mathbf{n}_{\min}$

$$\bar{I} = \{k \mid (\mathbf{n}_k \cdot \mathbf{n}_{\min}) < 0\}. \tag{17}$$

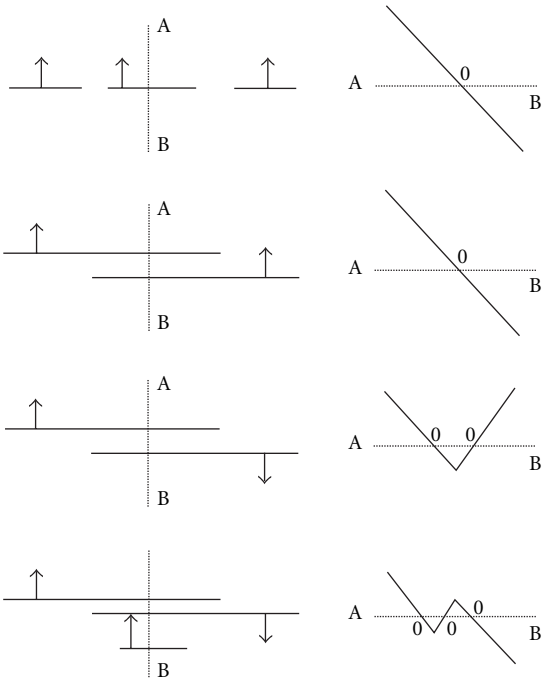

Figure 3: Distance function in the case of multiple surfaces. Left: surface sections with the relative normals. Right: distance profile along section A-B.

At this point we can determine $d_{\text{opp}}(\mathbf{x})$ as the distance with minimum magnitude among those that are oriented opposite to $\mathbf{n}_{\min}$ and use this value as a threshold to rule out of I all distances whose magnitude is greater than $d_{\text{opp}}(\mathbf{x})$. We can thus compute $d(\mathbf{x})$ as a linear combination of the remaining points of the set I

$$d(\mathbf{x}) = \sum_{i \in I} w_i d_i(\mathbf{x}), \tag{18}$$

where w_i are properly chosen weights.

In Figure 3, we can see some examples of distance profiles corresponding to uniform weights w_i. As a matter of fact, the choice of the weights w_i can be critical for a fine tuning of the result, as they allow to decide whether to trust one surface patch better than another one. Indeed, if we had a priori information on the accuracy and the reliability of a partial reconstruction, it would be easy to use this information through a careful choice of the weights. In our case, however, this information is not available. However, we can always infer an appropriate weight configuration on a heuristic basis. For example, if we are using an image-based depth estimation technique to obtain the partial reconstructions (range images), we can safely assume that the least reliable surface portions are those that lie in the proximity of self-occlusions or extremal boundaries. It is thus reasonable to assign a higher weight to regions that are far from the border. Another reasonable criterion can be used whenever the overlap involves several surfaces. In this case it is reasonable to limit the averaging only to those surfaces that remain within a certain distance from each other. This tends to rule out possible outliers in the partial reconstructions. One final possible parameter that could be easily considered in the computation of the distance function is surface orientation. In fact, if we knew the viewpoint associated to a certain partial reconstruction, we could decide to favor those surface areas that are more orthogonal to the viewing direction.

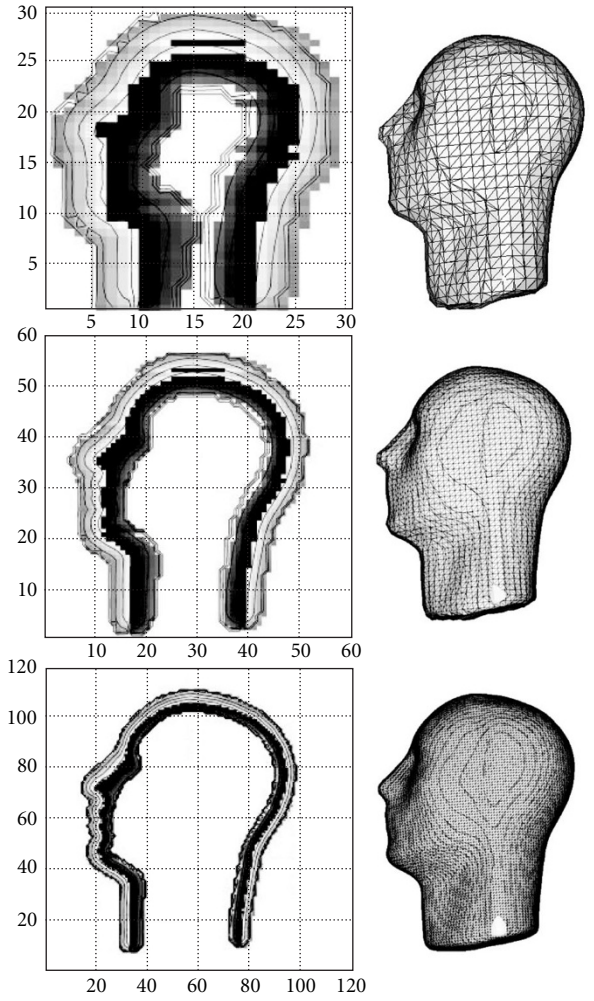

Figure 4: Multiresolution progression of the voxset where the volumetric function is defined.

3.3. Multiresolution

In order to obtain high performance at low computational cost, besides updating the volumetric function just in a narrow region around the zero level set (narrow-band implementation), we operate in a multiresolution fashion (see Figure 4). This can be achieved by starting with a low-resolution voxset and letting the front settle down. Then we break down the voxels around the propagating front and resume the front propagation. The operation continues until the final resolution is reached. Every time the voxset is split we proceed with a reinitialization of the newly introduced samples, which is done through simple linear interpolation.

Of course, we also need to recompute the distance function through an iterative process that is similar to the one used for the reinitialization of the narrow band (see Section 2.3).

The initial resolution must be set in such a way to be able to obtain a fast front evolution, without missing surface details. In fact, the voxel size should be decided in such a way to guarantee a correct sampling of all scene elements of interest. Failing to do so would result in a front that "passes through" some surface elements.

A key aspect of this process is the fact that the velocity field that drives the implosion of the level set can be precomputed on a hierarchical data structure (octree that best fits the available range data).

The resulting model is bound to be a set of closed surfaces, therefore all the modeling holes left after mosaicing the partial reconstructions are closed in a topologically sound fashion. In fact, those surface portions that cannot be reconstructed because they are not visible, can sometimes be patched up by the fusion process. This ability to mend the holes can also be exploited in order to simplify the 3D acquisition session, as it allows to skip the retrieval of some depth maps.

An interesting aspect of our fusion method is in the possibility to modify the surface characteristics through a processing of the volumetric function. For example, filtering the volumetric function results in a smoother surface model. Finally, the method exhibits a certain robustness against orientation errors, as the non perfect matching of surface borders can be taken care of by the fusion process through a careful definition of the distance function used in the specification of the volumetric motion field.

3.4. Examples of application

In order to test the effectiveness of the proposed technique, we applied it to a variety of study cases. A series of tests on synthetic data were conducted to confirm the system's ability to deal with complex topologies, with multiple objects, with facing surfaces, and with hole-mending situations. In particular, some tests on multiple facing surface were conducted on the synthetic data set (the handle of a pitcher chained to a torus), proving that the definition of the distance function for multiple surfaces, provided in Section 3.2, is effective (see Figure 5).

A particularly interesting experiment was conducted on a real object with a nontrivial topology (a bottle with a handle) that could easily create problems of ambiguities. Any traditional surface fusion approach would, in fact, encounter difficulties in deciding how to complete (close) the surface in the regions of missing data. Furthermore, besides exhibiting self-occlusion problems, this object puts the multiresolution approach under a severe test. We acquired six depth maps and assembled them together using an ICP algorithm [28] (see Figure 6). The result was an incomplete model with some accuracy problems in the overlapping regions (at the boundaries of the depth maps). The front evolution is shown in Figure 7, which results in the final model of Figure 8.

As we can see, the topology of the object is retrieved correctly, without having to provide the system with specific instructions. Also, through a simple low-pass filtering of the volumetric function, we can reduce the problems that otherwise would arise from the jaggedness of the borders of the surface patches.

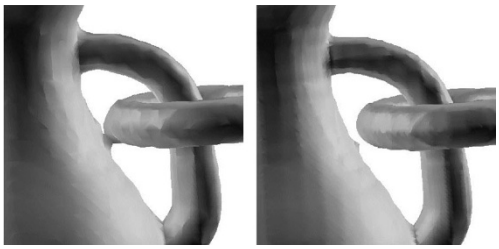

Figure 5: Testing the distance function: progressive reconstruction of a surface of complex topology with multiple facing surfaces.

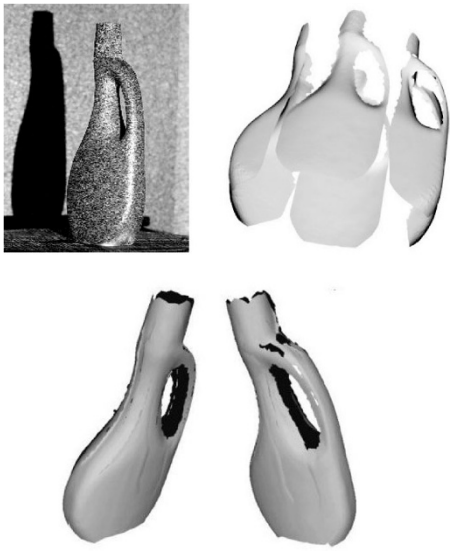

Figure 6: One of the original views (top left). Six unregistered surface patches obtained with stereometric techniques (top right). Two views of the assembled surface patches after registration (bottom): notice the creases due to a nonperfect model overlapping, and the presence of holes in the global model.

4. DIRECT SURFACE MODELING

In alternative to using 3D data for the generation of the complete closed object surface, we can directly use the available images. An image-based 3D modeling method that uses an implicit representation of surfaces was recently proposed by Faugeras and Keriven [29]. With this modeling approach the front evolves by following a motion that is always locally normal to the surface, with a speed that depends on the local surface curvature and to a measurement of the local texture mismatch between imaged and transferred textures. Transferring the imaged texture onto another view means back-projecting it onto the model and re-projecting it onto the other view. Our solution significantly improves this approach as, besides

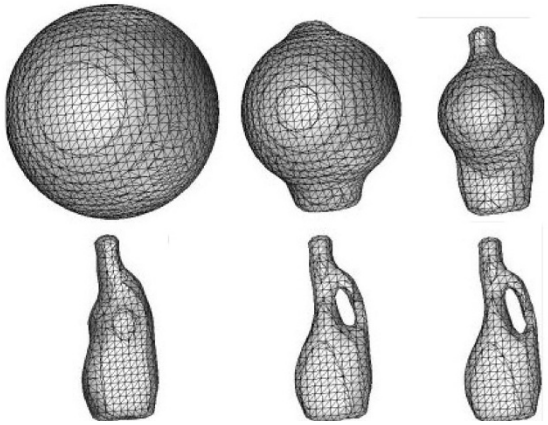

Figure 7: Level set implosion.

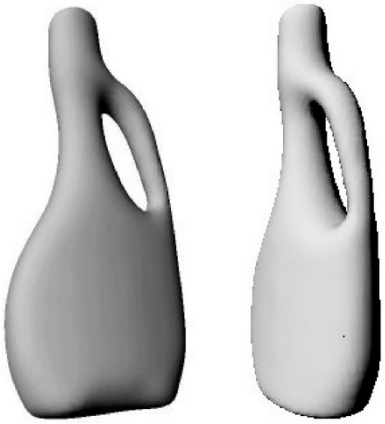

Figure 8: Final 3D model.

working on a narrow band around the evolving front, it operates in an adaptive multiresolution fashion, which boosts up the computational efficiency. Multiresolution, in fact, enables to quickly obtain a rough approximation of the objects in the scene at the lowest possible voxset resolution. Successive resolution increments allow to progressively refine the model and add details. In order to do so, we introduce several novel action terms in the velocity function, which allow to control the front evolution in the desired fashion. For example, we introduce "inertia" in the level set evolution, which tends to favor topological changes (e.g., the creation of doughnut-like holes in the structure). Other mechanisms that implement some sort of biased quantization and hysteretic evolution tend to prevent its dynamics from missing details (surface creases, ridges, etc.) at lower resolution levels, or to recuperate them at every resolution increment.

4.1. Definition of the velocity function

One of the terms that contribute to steering the level set evolution is the texture mismatch between imaged and transferred textures [24, 25], which is a function of the correlation between homologous luminance profiles [29]. The texture mismatch is

$$C(S,\mathbf{n}) = \int_S \psi(S,\mathbf{n},v,w)\,|\mathbf{s}_v \times \mathbf{s}_w|\,dv\,dw, \tag{19}$$

$$\psi = 1 - \sum_{i,j=1;\,i\neq j}^{n} \frac{1}{|I_i|\,|I_j|}\langle I_i, I_j\rangle, \tag{20}$$

where $\mathbf{d}\sigma = |\mathbf{s}_v \times \mathbf{s}_w|dvdw$ is the infinitesimal area element of the surface S, associated to the local surface parametrization (v, w) induced by the image coordinate chart; $\mathbf{n}$ is the surface normal; and $I_i(\mathbf{m}_i)$ is the luminance of pixel $\mathbf{m}_i$ in the ith image. This definition of $\mathbf{d}\sigma$ guarantees that the surface representation will be independent of the variables (u, w). The surface patch S through which the luminance transfer occurs is assumed to be a locally planar approximation of the propagating front. Indeed, in order to guarantee that this approximation will maintain a constant quality, the size of this planar patch will change according to the local curvature of the level set.

The inner product (correlation) between the pair of subimages I_i and I_j is defined as follows:

$$\langle I_i, I_j\rangle = \frac{1}{4pq}\int_{-p}^{p}\int_{-q}^{q} (I_i(\mathbf{m}_1+\mathbf{m}) - \overline{I_i}(\mathbf{m}_1)) \times (I_j(\mathbf{m}_2+\mathbf{m}) - \overline{I_j}(\mathbf{m}_2))\mathbf{dm}, \tag{21}$$

where $\mathbf{m}_1$ and $\mathbf{m}_2$ are homologous image points (i.e., image points that correspond to the same point of the surface model), and

$$\overline{I_k}(\mathbf{m}_k) = \frac{1}{4pq}\int_{-p}^{p}\int_{-q}^{q} I_k(\mathbf{m}_k+\mathbf{m})\mathbf{dm}, \quad k = 1, 2. \tag{22}$$

Although the correlation could be computed between all the viewpoints where there is visibility, only the pair of views with the best visibility is considered. Visibility can be easily checked through a ray-tracing algorithm and measured as a function of the angle between visual ray and surface normal. Notice that normalizing the correlation has a twofold purpose: to limit its range between 0 and 2; and to guarantee that low energy areas (smooth texture) will have the same range of high energy (rough texture) areas. Finally, subtracting the average from a luminance profile tends to compensate a non-Lambertian behavior of the imaged surfaces.

In order to achieve the desired front evolution, we propose and define a novel velocity function that mediates the twofold need of guaranteeing surface smoothness and consistency between images and final model

$$F(\mathbf{x}) = C(\mathbf{x})\mathrm{div}\phi + \nabla\psi\cdot\nabla\phi + \alpha\psi. \tag{23}$$

Texture-curvature action

The first term $C(\mathbf{x})\,\mathrm{div}\,\phi$ of (23), where $\mathrm{div}\,\phi = \nabla\cdot\nabla\phi$, represents the texture-curvature action and favors a maximally smooth implosion toward a shape that agrees with the available textures. The presence of the texture mismatch cost C, in fact, tends to slow down areas with modest cost, and speed up areas of high cost.

Hook-on action

Ideally, we would be lead to think that the first term is sufficient to correctly steer the model's evolution, as correct surface regions should have a zero cost, while other regions are left free to evolve. This, however, is not really true as the cost is rarely equal to zero due to a nonperfect luminance transferral (a homography models just a first-order approximation of the surface) and a non-Lambertian radiometric behavior. Because of that, without some additional contrasting action, the front propagation would "trespass" the correct surface and continue its evolution uncontrollably. The second term of (23) will tend to contrast this behavior. In fact, in the proximity of the actual surface, the local cost gradient $\nabla\psi$ is almost parallel (although oppositely oriented) to the propagation front's normal $\mathbf{n} = \nabla\phi$. As a consequence, $\nabla\psi \cdot \nabla\phi < 0$ tends to stabilize the front in the proximity of the actual surface. Furthermore, this term exhibits the desirable property of speeding up the evolution of the front in the proximity of configurations of minimum cost, as it accounts of a positive action $\nabla\psi \cdot \nabla\phi > 0$.

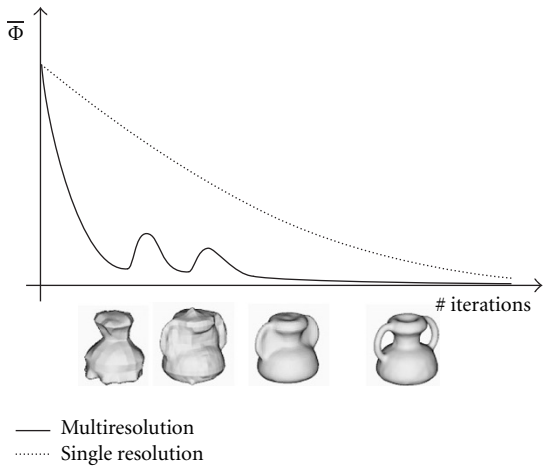

Figure 9: Illustration of the temporal evolution of the cost function (texture mismatch) and of the model. Notice that the cost value suddenly increases at every resolution change, due to the mechanism of recovery of details.

Inertia action

The third term of (23) acts like an "inertial" term in order to favor concavities in the final model. The weight factor $\alpha > 0$ is constant all over the front, but it is variable in time. In fact, α must satisfy two opposite needs: on one hand its magnitude needs to be small enough to avoid affecting the action of the first term of (23); on the other hand, it has to be large enough to produce the desired topological changes. We found experimentally that a good choice for α corresponds to the average curvature of the front at every time step

$$\alpha = \frac{\int_S |\mathrm{div}\phi| d\sigma}{\int_S d\sigma}. \tag{24}$$

The weight α needs to be rather frequently updated, sometimes at every iteration. However, this operation does not require additional computational effort, as the first action term of (23) already requires the computation of $\mathrm{div}\,\phi$.

4.2. Multiresolution

If the volumetric function that characterizes the level set is defined on a static voxset of $N \times N \times N$ voxels, the computational complexity of each front propagation step is proportional to N^2, as it is proportional to the surface of the level set (narrow-band computation). Furthermore, since the velocity F is multiplied by $|\nabla\psi|$ (which is equal to the sampling step), the number of iterations turns out to be proportional to N, with a resulting algorithmic complexity that is proportional to N^3. In order to dramatically reduce this complexity, we developed a multiresolution approach to level set evolution. The algorithm starts with a very low resolution level (a voxset of 10–15 voxels per side). When the propagation front converges, the resolution increases and the front resumes its propagation. The process is iterated until we reach the desired resolution. A progressive resolution increment has the desired result of minimizing the amount of changes that each propagation step will introduce in the model, with the result of achieving a better global minimum of the cost function. Furthermore, the number of iterations will be dramatically reduced (from N to $\log N$) with respect to a fixed-resolution approach, with an algorithmic complexity that turns out to be proportional to $N^2 \log N$.

Indeed, starting from a low-resolution voxset, we need to prevent the algorithm from losing details at that resolution or to make sure that the algorithm will be able to recover the lost details. In fact, we have to keep in mind that the motion by curvature tends to dominate over the other terms, therefore some of the details of the object may totally disappear. In order to prevent this from happening, we limit the impact of the local curvature on the front's evolution through a "soft" clipping function, which guarantees a better evolutional behavior than hard clipping.

In spite of this smooth thresholding mechanism, in some cases it is not possible to prevent some of the smaller details from disappearing. For this reason, we developed a technique that enables the recovery of lost details before the resolution is increased, which is based on a mechanism of hysteresis in the surface implosion. The idea is to keep track of all the voxels on the zero level set whose cost Ψ is below a certain threshold. After the implosion of the level set, we let the propagation front evolve while driven by a different cost function that depends on the distance between the surface and such points. This operation makes the surface literally "climb up" the lost details. As an example of applications, see Figure 9, which illustrates the temporal evolution of the cost function (texture mismatch) during a multiresolution front evolution. Notice that the cost value suddenly increases at every resolution change, due to the mechanism of recovery of details. The graph, however, confirms that the convergence of the cost function in the multiresolution case is much faster than in the single-resolution case.

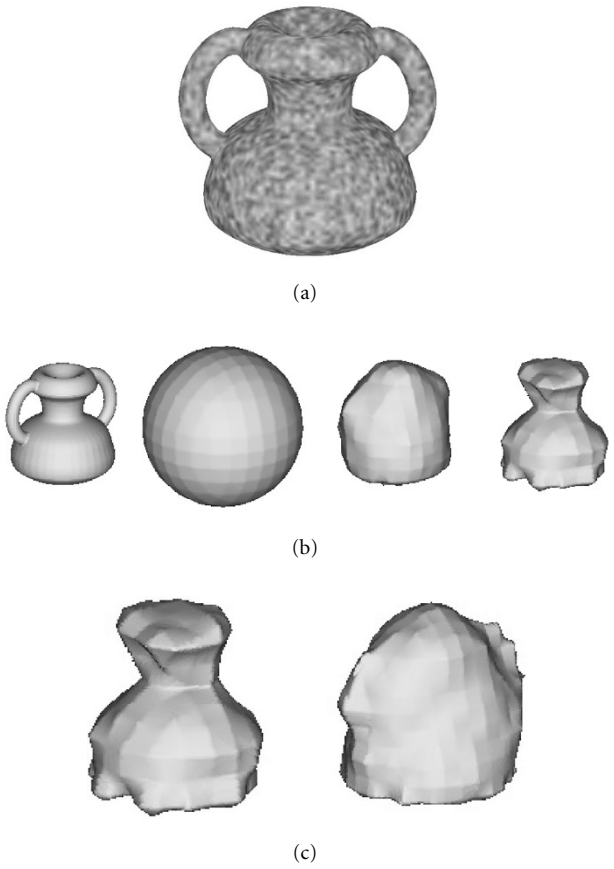

(a)

(b)

(c)

Figure 10: Detail recovery in an object with relevant small details of high curvature. Original image (a), evolution with no backtracking (b), backtracking re-expansion (c).

Two are the critical aspects associated to a resolution change: the management of resolution changes; and the recovery of lost details. The first problem can be approached with a simple interpolation with half the sampling step, followed by a low-pass filter. The second problem is far more complex, and deserves further discussion.

The basic idea is to select the minimum resolution that allows the front evolution to proceed, without worrying too much about lost details. The final resolution, of course, will depend on the accuracy of the details that we want to represent. Consider, for example, the object of Figure 10a, which exhibits relevant details of small size and high curvature. If we let a low-resolution level set ($10 \times 10 \times 10$ voxels) evolve under the influence of the above described velocity terms, we obtain the evolution shown in Figure 10b. The algorithm can initially sense the presence of the pitcher's handles, as the evolving front slows down in their proximity. The front, however, ends up missing the handles completely. This is mainly due to the curvature component of the velocity function, which tends to flatten the front. In fact, any detail whose curvature radius is smaller than the voxel size is filtered out by the front evolution. Roughly speaking, if the resolution is too low, the handles are treated like a ripple to be removed.

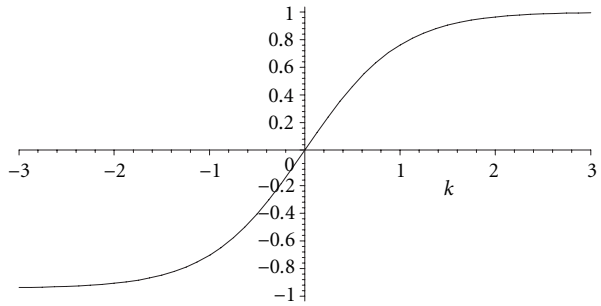

Figure 11: Plot of the soft thresholding function $\beta \tanh(k)$, with $\beta = 1$ (typical value for most applications).

We recall that the texture-curvature term in the velocity function is the product between texture mismatch ψ and the curvature $\nabla \cdot \nabla\phi$ of the front, therefore although the mismatch ψ becomes very small as the front passes through the handles, the curvature factor becomes very large, with the result that the corresponding velocity term does not become zero and the front continues to advance.

In order to avoid this problem, we limit the impact of the front's local curvature through a "soft clipping" function (see the hyperbolic tangent function of Figure 11). The value of β represents the limit we set for the curvature $k = \nabla \cdot \nabla\phi$, and it is usually set to 1.

Although this soft clipping process is effective in many situations, some complex topologies such as the one of Figure 10a, cannot be correctly reconstructed when starting from a coarse initial resolution. For this reason, we implemented a method for recuperating the lost details before a resolution change. The idea is to keep track of the coordinates of all the voxels of the zero level set where the texture mismatch ψ is lower than a certain threshold ε. It is quite reasonable to expect that this set $\mathcal{P}$ of points correspond to all details that have been missed at the previous resolution level. After the front evolution settles to an equilibrium configuration, the algorithm begins a backtracking phase in which the front expands toward the points of the set $\mathcal{P}$. In order to do so, we use such points as attractors by adding a new action term in the velocity function, which accounts for the distance from such points.

As we can see in Figure 10c, the point cloud $\mathcal{P}$ (here corresponding to the pitcher's handle) attracts the closest points of the front in order for the next implosion, which will occur at a higher resolution level, to begin from a model that contains all the previously lost details. In Figure 10c we can see the front evolution during the re-expansion phase.

4.3. Implementational issues

In order to maximize the computational efficiency of the proposed algorithm, we devised and adopted a number of solutions. For example, we implemented some mechanisms for recognizing whether the front evolution has locally converged to a stationary solution. In that case, we mark the stationary subregions as fixed until the next resolution changes.

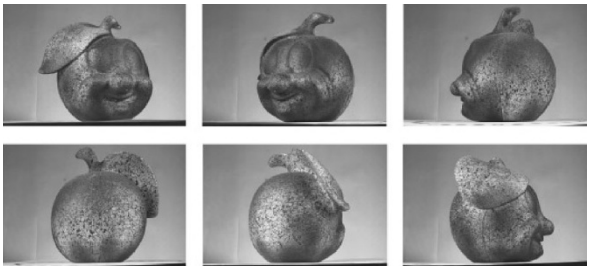

Figure 12: Sequence of original views.

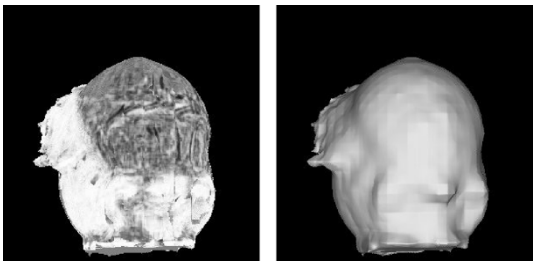

Figure 13: A view of the cost function mapped onto the propagation front. The darker the texture is, the heavier the mismatch.

This operation alone results in a saving of about 50% of the total computational time. Significant computational savings also arise from the choice of computing the luminance agreement only on two images at a time ($n = 2$ in (20)) [14].

As for the algorithmic automaticity, we devised and implemented a number of solutions that reduce the intervention of the operator to a minimum. For example, the algorithm selects, for each surface point, the best pair of cameras (C_1, C_2) for the computation of the correlation (21). This is done by selecting the cameras whose viewing direction is most parallel to the surface normal and whose view of the point is not occluded.

Another important problem to assess is the choice of the width of the window used for computing the correlation between textures. In fact, in order to keep computational complexity at a reasonable level, luminance transfer between views is performed through the local tangent plane to the surface (homography). This window cannot be too extended otherwise texture warping would come in the way, but it cannot be too small, otherwise we would have problems of matching ambiguity. What we did in our implementation is to link the window size to the radius of curvature of the evolving front through a simple proportionality relationship. In fact, the radius of curvature ρ can be derived immediately as the reciprocal of the divergence of the volumetric function.

4.4. Examples of application

In order to prove the effectiveness of our approach to 3D modeling, we tested it on several objects acquired with a camera moving around them. In this section, we show the results in two different cases characterized by a significantly

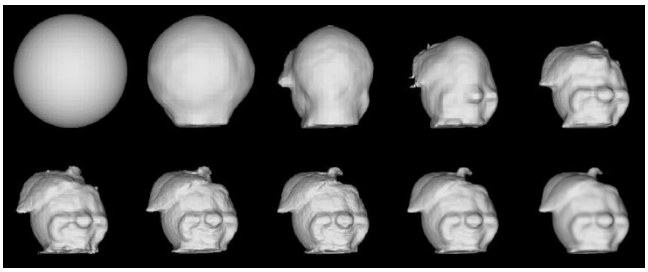

Figure 14: Temporal evolution of the propagation front. The initial volumetric resolution is very modest (in this case the voxset size is $20 \times 20 \times 20$), and is not able to account for some topologically complex details of the surface (the fifth frame in lexicographic order is the best one can do at this resolution). As the resolution increases, more details begin to appear, such as the stem of the apple.

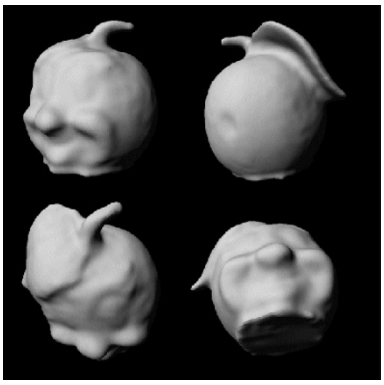

Figure 15: Four views of the final 3D model.

complex topology. The first test concerns a styrofoam object with fine natural texturing (see Figure 12). The images are acquired using a fixed CCIR B/W analog camera (720×576 pixels) pointed at the object while it rotates on a turntable. We used a subsampling of the whole sequence (one shot every 20 degrees of rotation), and we set the algorithm in such a way to evolve in three resolution stages. As we can see from Figure 13, the front evolution is well steered by the cost function. In fact high values of the cost (darker areas in the left image) correspond to regions where the surface is still far from a reasonable approximation of the actual surface. Figure 14 shows the temporal evolution of the propagating front, as the resolution changes. As we can see, details that are only roughly sketched at a lower resolution level, are better recovered at the next resolution level. In Figure 15 we can see how the algorithm was able to carve the surface even under the leaf and recover hidden topological details at later stages of the front evolution. We also tested our algorithm with a sculpture that exhibited only a modest local texturing (see Figure 16). In this case we used a digital camera with a resolution of 1500×1000 pixels that acquired the subject in similar conditions as the previous case (one shot every 20 degrees, three resolution stages). As we can see from Figures 17 and 18, once again the method proved to be remarkably robust against topological complexity. We also

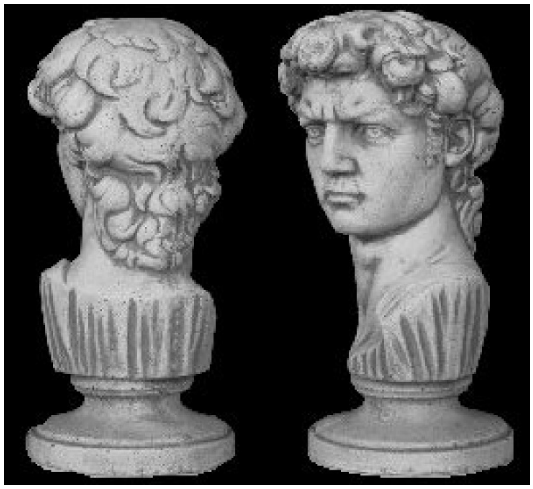

FIGURE 16: Two of the original views of the subject.

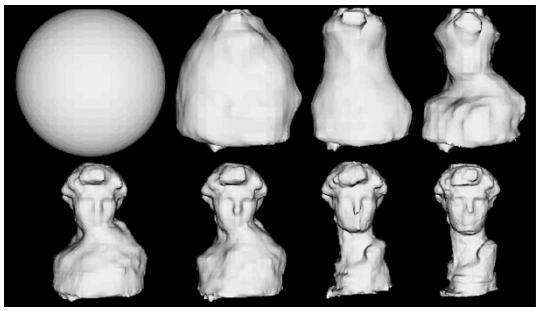

FIGURE 17: Temporal evolution of the propagation front.

performed some experiments in which the images were acquired with a modestly cluttered background, without significantly affecting the evolution of the front.

5. CONCLUSIONS

In this paper we discuss two image-based 3D modeling methods based on a multiresolution evolution of a volumetric function's level set. The first consists of fusing ("sewing" and "stitching") numerous partial reconstructions (depth maps) into a closed model, while the second consists of steering the level set's implosion with texture mismatch between views. Both solutions share the characteristic of operating in an adaptive multiresolution fashion, which boosts up computational efficiency and robustness.

Both modeling applications have been written in C++, and run on several SW platforms. Computational times depend on the final resolution and on the topological complexity of the imaged object. Using a PC equipped with a Pentium III 800 MHz with a 256 MB RAM, the fusion algorithm always completes its task in just a few minutes on voxsets of $128 \times 128 \times 128$ voxels. A bit more intensive is the direct approach, mostly because none of the computation can be done in advance. In this case, although the implementation is not optimized, we need less than 10 minutes per resolution level.

FIGURE 18: Final 3D model. The rendered view is here blended with a model's wireframe, obtained after mesh simplification.

We are currently working on a new version of the above methods, based on 3D mesh adaptivity, which will further improve the computational efficiency and the effectiveness of the solution. We are also working on an image-based automatic fine tuning of the algorithm's parameters.

REFERENCES

[1] R. Hartley and A. Zisserman, *Multiple View Geometry in Computer Vision*, Cambridge University Press, Cambridge, UK, 2000.

[2] A. Dell'Acqua, A. Sarti, and S. Tubaro, "Effective analysis of image sequences for 3D camera motion estimation," in *Intl. Conf. on Augmented, Virtual Environments and Three-Dimensional Imaging (ICAV3D 2001)*, Mykonos, Greece, 30 May–1 June 2001.

[3] A. Azarbayejani and A. Pentland, "Recursive estimation of motion, structure, and focal length," *IEEE Trans. on Pattern Analysis and Machine Intelligence*, vol. 17, no. 6, pp. 562–575, 1994.

[4] J. A. Sethian, *An analysis of flame propagation*, Ph.D. thesis, Department of Mathematics, University of California, Berkeley, Calif, USA, 1982.

[5] J. A. Sethian, *Level Set Methods and Fast Marching Methods*, Cambridge University Press, Cambridge, UK, 2nd edition, 1996.

[6] V. Caselles, F. Catte, T. Coll, and F. Dibos, "A geometric model for active contours in image processing," *Numer. Math.*, vol. 66, no. 1, pp. 1–31, 1993.

[7] R. Malladi and J. A. Sethian, "A unified approach for shape segmentation, representation and recognition," Tech. Rep. 614, Center for pure and applied mathematics, University of California, Berkeley, Calif, USA, 1994.

[8] R. Malladi and J. A. Sethian, "Image processing via level set curvature flow," *Proc. Nat. Acad. Sci. U.S.A.*, vol. 92, pp. 7046–7050, July 1995.

[9] R. Malladi and J. A. Sethian, "Level set methods for curvature flow, image enhancement, and shape recovery in medical images," in *Visualization and Mathematics*, pp. 329–345, Springer-Verlag, Heidelberg, Germany, June 1995.
[10] R. Malladi, J. A. Sethian, and B. C. Vemuri, "Shape modeling with front propagation: A level set approach," *IEEE Trans. on Pattern Analysis and Machine Intelligence*, vol. 17, no. 2, pp. 158–175, 1995.
[11] R. Malladi and J. A. Sethian, "A unified approach to noise removal, image enhancement, and shape recovery," *IEEE Trans. Image Processing*, vol. 5, no. 11, pp. 1554–1568, 1996.
[12] R. Malladi, J. A. Sethian, and B. C. Vemuri, "A fast level set based algorithm for topology-independent shape modeling," *J. Math. Imaging Vision*, vol. 6, no. 2/3, pp. 269–290, 1996.
[13] R. Malladi and J. A. Sethian, "Level set and fast marching methods in image processing and computer vision," in *Proc. IEEE International Conference on Image Processing*, Lausanne, Switzerland, September 1996.
[14] R. Keriven, *Equations aux Dérivées Partialles, Evolution de Courbes et de Surfaces et Espaces d'Echelle: Applications à la Vision par Ordinateur*, Ph.D. thesis, École Nationale des Ponts et Chaussées, Paris, France, 1997.
[15] A. Sarti and S. Tubaro, "A multiresolution level-set approach to surface fusion," in *Proc. IEEE International Conference on Image Processing*, Thessaloniki, Greece, October 2001.
[16] A. Colosimo, A. Sarti, and S. Tubaro, "Image-based object modeling: a multiresolution level-set approach," in *Proc. IEEE International Conference on Image Processing*, Thessaloniki, Greece, October 2001.
[17] S. Osher and J. A. Sethian, "Fronts propagating with curvature dependent speed: Algorithms based on Hamilton-Jacobi formulations," *J. Computational Phys.*, vol. 79, no. 1, pp. 12–49, 1988.
[18] R. Malladi and J. A. Sethian, "An $O(N \log N)$ algorithm for shape modeling," *Proc. Nat. Acad. Sci. U.S.A.*, vol. 93, no. 18, pp. 9389–9392, 1996.
[19] M. Sussman, P. Smereka, and S. Osher, "A level set approach for computing solutions to incompressible two-phase flow," *J. Computational Phys.*, vol. 114, pp. 146–159, 1994.
[20] M. Sussman and E. Fatemi, "An efficient, interface preserving level set re-distancing algorithm and its application to interfacial incompressible fluid flow," *SIAM Journal on Scientific Computing*, vol. 20, no. 4, pp. 1165–1191, 1999.
[21] R. Keck, *Reinitialization for Level Set Methods*, Dipl. thesis, University of Kaiserslautern, Department of Mathematics, Kaiserslautern, Germany, June 1998.
[22] D. Adalsteinsson and J. A. Sethian, "The fast construction of extension velocities in level set methods," *J. Computational Phys.*, vol. 148, no. 1, pp. 2–22, 1999.
[23] W. E. Lorensen and H. E. Cline, "Marching cubes: A high resolution 3D surface construction algorithm," *Computer Graphics (Proc. SIGGRAPH '87)*, vol. 21, no. 4, pp. 163–169, 1987.
[24] P. Pigazzini, F. Pedersini, A. Sarti, and S. Tubaro, "3D area matching with arbitrary multiview geometry," *Signal Processing: Image Communication*, vol. 14, no. 1-2, pp. 71–94, 1998.
[25] F. Pedersini, A. Sarti, and S. Tubaro, "Multi-resolution 3D reconstruction through texture matching," in *European Signal Processing Conference (EUSIPCO-2000)*, vol. 4, pp. 2093–2096, Tampere, Finland, September 2000.
[26] F. Pedersini, A. Sarti, and S. Tubaro, "Visible surface reconstruction with accurate localization of object boundaries," *IEEE Trans. Circuits and Systems for Video Technology*, vol. 10, no. 2, pp. 278–291, March 2000.
[27] F. Pedersini, P. Pigazzini, A. Sarti, and S. Tubaro, "Multicamera motion estimation for high-accuracy 3D reconstruction," *Signal Processing*, vol. 80, no. 1, pp. 1–21, 2000.
[28] P. J. Besl and N. D. McKay, "A method for registration of 3-D shapes," *IEEE Trans. on Pattern Analysis and Machine Intelligence*, vol. 14, no. 2, pp. 239–256, 1992.
[29] O. Faugeras and R. Keriven, "Variational principles, surface evolution, PDE's, level set methods, and the stereo problem," *IEEE Trans. Signal Processing*, vol. 7, no. 3, pp. 336–344, 1998.

Augusto Sarti was born in Rovigo, Italy, in 1963. He received the "laurea" degree (Summa cum Laude) in Electrical Engineering in 1988 and the Ph.D. degree in electrical engineering and information sciences in 1993, both from the University of Padua, Italy. He spent two years doing research on nonlinear system theory at the University of California, Berkeley. Prof. Sarti is currently an Associate Professor at the Politecnico di Milano, Italy and his research interests are mainly in digital signal processing and, in particular, computer vision, image analysis, audio analysis, and processing and rendering.

Stefano Tubaro was born in Novara in 1957. He completed his studies in Electronic Engineering at the Politecnico di Milano, Italy, in 1982. He then joined the Dipartimento di Elettronica e Informazione of the Politecnico di Milano, first as a researcher of the National Research Council, and then (in November 1991) as an Associate Professor. His current research interests are on image and video analysis for the geometric and radiometric modeling of 3D scenes; advanced algorithms for video coding and sound processing. Stefano Tubaro authored more than 80 scientific publications on international journals and congresses. He also coauthored two books on digital processing of video sequences. Stefano Tubaro coordinates the research activities of the image and sound processing group (ISPG) at the Dipartimento di Elettronica e Informazione of the Politecnico di Milano, which contributed to numerous national projects and several european research projects.